A Dual-band Monopole Antenna with EBG for Wearable Wireless Body Area Networks

Chao Wang [1], Liang Zhang [2*], Shenbing Wu [1], Shijie Huang [1], Changqing Liu [1], and Xianliang Wu [1]

[1] Key Lab of Ministry of Education of Intelligent
Computing & Signal Processing, Anhui University, Hefei City, China
P18201026@stu.ahu.edu.cn, P18201031@stu.ahu.edu.cn, P18201028@stu.ahu.edu.cn,
P18201024@stu.ahu.edu.cn, xlwu@ahu.edu.cn

[2] AnHui Province Key Laboratory of Simulation and Design
Electronic Information System, Hefei Normal University, Hefei City, China
liangzh@hfnu.edu.cn

Abstract ─ This paper proposes a dual-band wearable monopole antenna adopting an electromagnetic band-gap (EBG) structure, which operates at 2.45 and 5.8 GHz ISM bands and is suitable for wearable applications. Both the monopole antenna and the EBG structure are fabricated on an F4B semi-flexible substrate having a dielectric constant of 2.2. The EBG structure effectively isolates the human body from the radiation of the antenna and reduces the specific absorption rate (SAR) of it by more than 97.5%. This improves the antenna gain and the peak gain reaches 9.1 dBi at 5.8 GHz. The wearable performance of the antenna showed that it can sustain good performance even under realistic human body loading. Besides, the antenna has a small size, which makes it ideal for wearable applications.

Index Terms ─ Dual-band, EBG structure, low SAR value, wearable antenna.

I. INTRODUCTION

In the last decade, wireless body area networks (WBAN) received significant attention from the researchers, and several applications, such as elderly/ child health monitoring, battlefield search and rescue, and wearable watches, aroused [1-2]. As one of the communication bands of the WBAN system, publicly available 2.40-2.48 and 5.725-5.875 GHz scientific, industrial, and medical (ISM) bands are assigned.

Wearable antennas for WBAN applications require placement on the human body, which necessitates body-related factors, such as bending deformation and high loss to be taken into account during the design process [3]. Furthermore, to avoid the potential impact of radiation on human health, the SAR value of antennas has to be minimized [4]. The literature has several designs of wearable antennas, where planar inverted F antennas [5], monopole antennas [6-8], and microstrip antennas [9-10] have been proposed for wearable applications to achieve reasonable bending robustness. However, due to their nearly omnidirectional radiation characteristics, a large amount of electromagnetic energy radiation penetrates the human body. Currently, isolating the radiation of the antenna to the human body and reducing the SAR value are challenging issues [11]. A common method is to introduce an EBG structure [12-19] into the wearable antenna design, thereby achieving the purpose of separating the antenna radiation from the human body, and greatly reducing the SAR value of the antenna. However, the use of EBG also brings other drawbacks, such as increment in the antenna size and narrower impedance bandwidth.

This paper proposes a dual-band monopole wearable antenna with an EBG structure. The wearable antenna has small size and high gain characteristics compared to the configurations in Table 4 reporting wearable applications, which are applied to WBAN covering two ISM bands: 2.40-2.48 GHz and 5.725-5.875 GHz. Among them, the 2.45 GHz impedance bandwidth is 3.70% (2.40-2.49 GHz), where the 5.8 GHz impedance bandwidth reaches 28.9% (4.85-6.49 GHz). The EBG structure can significantly reduce the SAR value of the monopole antenna by more than 97.5%. Besides, the monopole antenna combined with EBG can still maintain good performance during human loading. These characteristics make the antenna suitable for wearable applications.

II. ANTENNA AND EBG DESIGN

A. Antenna design

This paper proposes a dual-band wearable monopole

Submitted On: September 16, 2020
Accepted On: November 30, 2020

https://doi.org/10.47037/2020.ACES.J.360107

antenna with an EBG structure. The design dielectric constant of 2.2 and a loss tangent of 0.007. It is fed by a coplanar waveguide (CPW). Figure 1 (a) shows the structure parameters of the antenna. The antenna was simulated using the electromagnetic simulation software HFSS 2019. The final design values of the proposed antenna are as follows: W = 26, W_1 = 22.4, Ws = 10.85, L = 26, L_1 = 13.7, L_2 = 12.5, R = 5.5, Wf = 3.3, g = 0.5, Le = 22.57, L_m = 21.57, L_n = 13.07, $d_1 = d_2$ = 1.5, h = 7, Ls = 12, s = 2.25, ss = 0.5 (unit: mm).

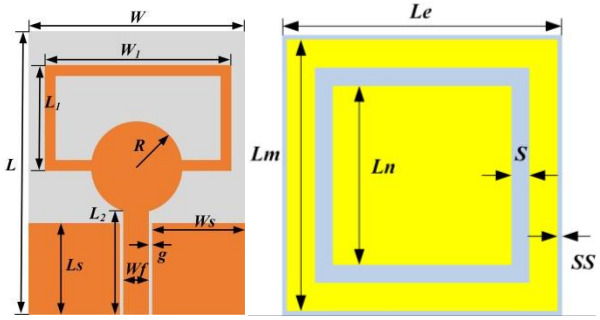

(a) (b)

Fig. 1. Configuration of (a) monopole antenna and (b) EBG unit.

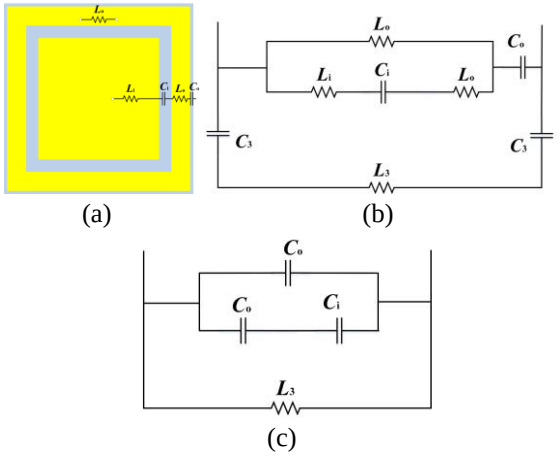

(a) (b) (c)

Fig. 2. Equivalent circuit of EBG: (a) equivalent capacitance and inductance, (b) equivalent circuit diagram, and (c) simplified equivalent circuit diagram.

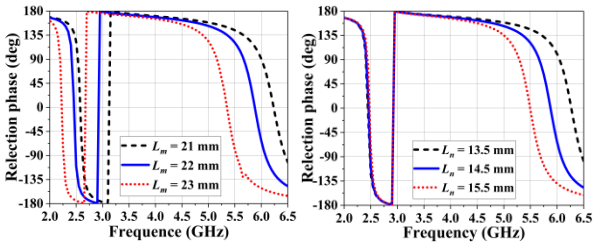

(a) (b)

Fig. 3. Influence of the EBG structure parameters on the reflection phase: (a) *Lo*; (b) *Li*.

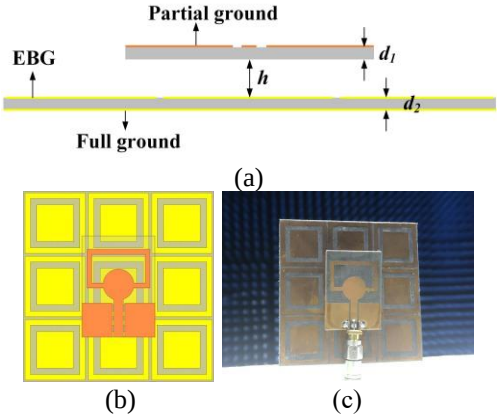

(a)

(b) (c)

Fig. 4. Configuration of the antenna with the EBG structure: (a) cross-sectional view, (b) top view, and (c) prototype measured.

B. EBG design

The high-impedance EBG structure is obtained by periodically arranging the metal patches on a dielectric substrate, where the patches can be of various shapes. As the frequency changes, the impedance of the EBG surface shows a $0 \rightarrow \infty \rightarrow 0$ behavior, which is $180° \rightarrow 0° \rightarrow -180°$ for the reflected phase. When the reflected phase θ is $\pm 180°$, the EBG surface impedance gets closer to 0, which is equivalent to the surface of a perfect electrical conductor (PEC). The phase of the reflected electromagnetic field is opposite to the phase of the incident electromagnetic wave. When the reflected phase θ is 0°, the surface impedance goes to infinite, and the phase of the reflected electromagnetic field is in-phase with the phase of the incident electromagnetic wave. At this time, the EBG surface exhibits an in-phase reflection. The frequency range of the $\pm 90°$ near the zero reflection phase belongs to the in-phase reflection area, while the other frequency ranges belong to the out-of-phase reflection area. Figure 1 (b) shows the geometry of the designed EBG unit. The frequency range of the reflected phase of the EBG unit $-90°$ to $+90°$, can be operated at 2.45 and 5.8 GHz ISM bands by adjusting the structural parameters.

Figures 2 (a) and (b) show the equivalent circuit diagram of the above-mentioned EBG structure to further explain its suppression effect on the surface waves. In these, C_o, C_i, and C_3 stand for the equivalent capacitances between the adjacent unit cells, the outer rectangular ring and the inner patch gap, and the top layer and the ground plane, respectively. Also, L_o and L_i respectively represent the equivalent inductance of the upper metal patch and the inner rectangular ring patch, where L_3 is the equivalent inductance of the ground plane

of the lower layer. Since the equivalent inductance of the upper surface of the EBG unit is much smaller than the equivalent capacitance, the series inductance-capacitance element can be equivalent to a single capacitance element. Furthermore, the capacitance C_3 can be ignored, and hence the equivalent circuit can be further simplified as shown in Fig. 2 (c). The surface impedance of the EBG can be expressed as:

$$Z = \frac{1}{j\omega C + \frac{1}{j\omega L_3}} = \frac{j\omega L_3}{1 - \omega^2 L_3 C}. \quad (1)$$

Then, the zero reflection phase point (θ = 0°) of the EBG is:

$$\omega = 2\pi f = \frac{1}{\sqrt{L_3 C}}. \quad (2)$$

Finally, the resonance frequency of the EBG is:

$$f = \frac{1}{2\pi\sqrt{L_3 C}}. \quad (3)$$

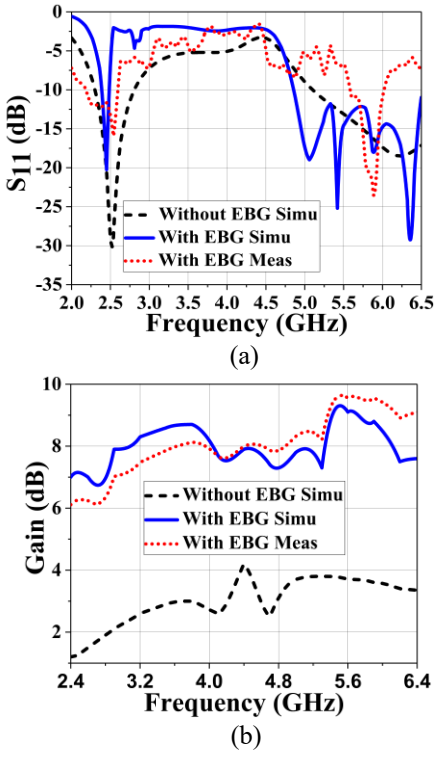

Fig. 5. Simulated performance of the antenna with and without the EBG structure and measured performance of the antenna with the EBG structure: (a) S11; (b) gain.

By incorporating (2) into (1), we can get: $Z \to \infty$, i.e., the surface impedance of the EBG goes to infinite. The EBG structure has two zero-phase reflection points: i) $C_L = C_o + C_i$ at the low frequency of 2.45 GHz, and ii) $C_H = C_o$ at the high frequency of 5.8 GHz. Hence, by designing the zero-phase point of the EBG near the resonant frequency of the antenna, the antenna performance can be improved.

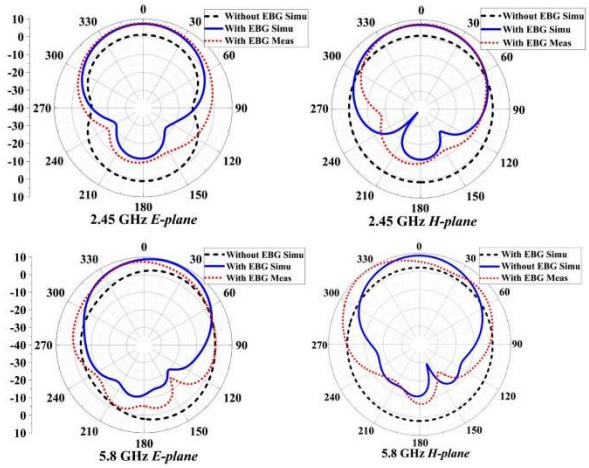

Fig. 6. The radiation pattern of the antenna in different frequency bands.

The outer and inner rectangles of the EBG unit determine the reflected phase resonance of the low and high frequencies, respectively. Here, adjusting the inner and outer rectangular parameters L_n and L_m can change the equivalent capacitances C_i and C_o. In this way, the resonance frequency of the EBG structure can be adjusted to work at 2.45 and 5.8 GHz. The effects of L_m and L_n on the reflection phase of the EBG structure are analyzed, and the results are shown in Fig. 3 (a) and Fig. 3 (b), respectively. The results indicated that L_m can control the resonance frequency of the low and high-frequency bands, and the EBG unit can be obtained to operate the isotropic reflection phase at 2.45 GHz by adjusting L_m. When L_n changes, only a large change occurs at high frequencies, where the 2.45 GHz band is almost unchanged, indicating that they have little influence on each other. Hence, by adjusting L_n, the EBG unit can obtain an isotropic reflection phase working at 5.8 GHz, thereby realizing the 2.45 and 5.8 GHz dual-band. The size of the final EBG structure is optimized to be 23 × 23 × 1.5 mm. Finally, the −90° to +90° reflection phase bandwidth of the EBG structure is 2.41-2.49 GHz and 5.66-6.07 GHz.

C. Antenna and EBG combination

Within the -90° to +90° reflection phase bandwidth of the EBG structure range, the reflected wave from the EBG will constructively interfere with the radiating wave in the free space. However, the practical array size needs to be determined since it is impossible to realize the simulated infinite array. Small size is generally desirable, however the resonating frequency of the microstrip antenna and EBG reflector changes, and the antenna does not operate adequately when the EBG array is too small. This is because the parasitic capacitance

between the antenna and the EBG array affects the performance of the whole structure [21]. Therefore, when determining the period of the EBG array, it is necessary to adjust the structural parameters of the EBG, the antenna, and the height between them to obtain the desired resonance point and achieve good impedance matching.

Table 1: Human tissue dielectric characteristics at 2.4 GHz [24]

Layer	Thickness	ε_r	Conductivity σ (S/m)
Skin	2	37.95	1.49
Fat	8	5.27	0.11
Muscle	23	52.67	1.77

Table 2: Human tissue dielectric characteristics at 5.8 GHz [24]

Layer	Thickness	ε_r	Conductivity σ (S/m)
Skin	2	35.14	3.717
Fat	8	4.955	0.29313
Muscle	23	48.49	4.9615

Figure 4 (a) illustrates the cross-sectional view of the antenna with the EBG structure, after the height adjustment, where the impedance matching is best when the antenna is placed 7 mm above the EBG. Figure 4 (b) shows the effect diagram after combination, where a 3×3 EBG array is selected considering the size of the EBG structure and the performance of the antenna with the EBG. When measuring the S_{11} and the radiation pattern, the gap between the antenna and the EBG is filled with foam to reduce losses and prevent any electrical contact, where Fig. 4 (c) depicts the measured prototype. Throughout the measures, the height of the foam and the position of the antenna were carefully measured to reduce the error. Subsequently, the S_{11} gathered by simulations and measurements are compared, and the results are given in Fig. 5 (a). It is observed that the antenna equipped with EBG has a bandwidth of 2.40-2.49 GHz in the low-frequency band, and 4.95-6.49 GHz in the high-frequency band, which can completely cover the 2.40-2.48 GHz and 5.725-5.875 GHz ISM bands. Figure 5 (b) compares the gain of the antenna with and without the EBG structure, which reveals that the EBG significantly increases the gain to a peak level of 9.1 dBi at 5.8 GHz. Finally, we observed that the simulations and the measurements are no big difference in antenna gain.

Figure 6 compares the simulated radiation patterns of the antenna with and without the EBG structure. Besides, the measured radiation patterns with the EBG structure is also compared. As shown, the radiation without the EBG is omnidirectional, i.e., a large number of electromagnetic signals will penetrate the human body. The addition of the EBG structure, however, enables the antenna to increase its front-to-back ratio (FBR) by 18.2 dB at 2.45 GHz and by 19.8 dB at 5.8 GHz. This makes the antenna unidirectional, significantly reducing the number of electromagnetic signals entering the human body. This phenomenon is highly desired in the design of wearable antennas. Figure 6 also shows that the simulated and measured radiation patterns are not quite different.

III. WEARABLE PERFORMANCE ANALYSIS

Due to the highly lossy characteristics of human tissue, the antenna performance is adversely affected when placed on the human body. As shown in Fig. 7, the antenna is placed on the arms, chest, and legs, and its reflection coefficient is measured by using a vector network analyzer. The results gathered are compared with the free space measurements. Figure 8 reveals that placing the antenna on the human body can achieve a good impedance matching, which allows 2.40-2.48 and 5.725-5.875 GHz ISM bands to be covered completely without effect on the antenna usage.

(a) (b) (c)

Fig. 7. The antenna with the EBG structure placed at different parts of a real human body: (a) arm; (b) chest; (c) leg.

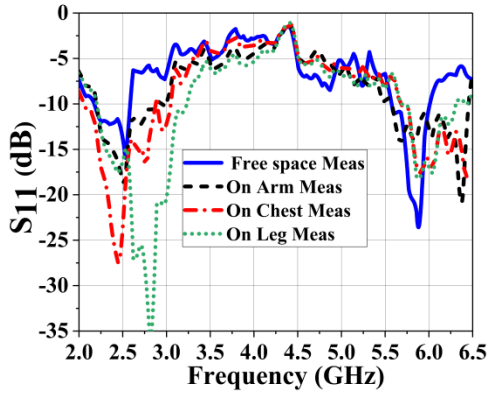

Fig. 8. Measured S_{11} of the antenna with the EBG on a real human body.

Table 3: SAR values of the antenna

With/Without EBG	1g/10g	Frequency (GHz)	Limit SAR (W/Kg)	Max SAR (W/Kg)	Input Power
Without EBG	1g	2.4	1.6	4.96	100mW
		5.8	1.6	10.9	100mW
	10g	2.4	2.0	2.6	100mW
		5.8	2.0	3.19	100mW
With EBG	1g	2.4	1.6	0.123	100mW
		5.8	1.6	0.212	100mW
	10g	2.4	2.0	0.0452	100mW
		5.8	2.0	0.0563	100mW

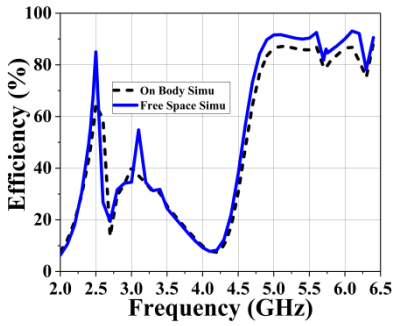

Fig. 9. Antennas simulate radiation efficiency on free space and human models.

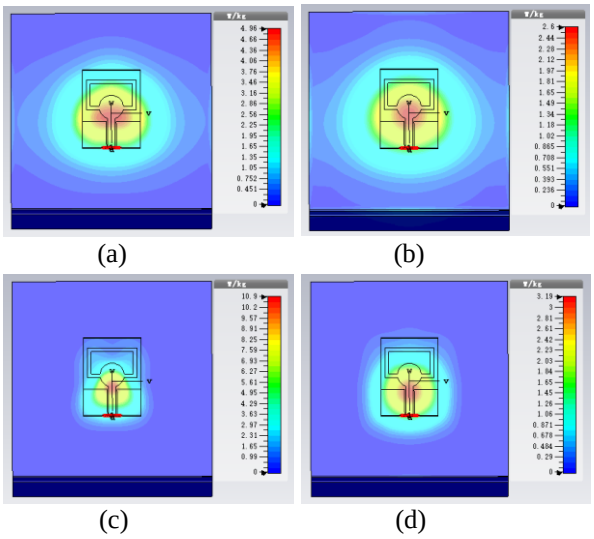

Fig. 10. Simulated SAR values for antennas without EBG. (a) 2.4 GHz, 1 g standard; (b) 2.4 GHz, 10 g standard; (c) 5.8 GHz, 1 g standard; (d) 5.8 GHz, 10 g standard.

In addition to the S_{11} analysis, the effect of the human tissue on radiation efficiency is also studied. Figure 9 shows the radiation efficiency of the antenna that is simulated for the free space and the human tissue model. The results reveal that the antenna achieves an efficiency of 64.6% at 2.45 GHz and 85.6% at 5.8 GHz without the human tissue model. When the human tissue model is added, the efficiency reduces to 53.2% at 2.45 GHz and 81.6% at 5.8 GHz.

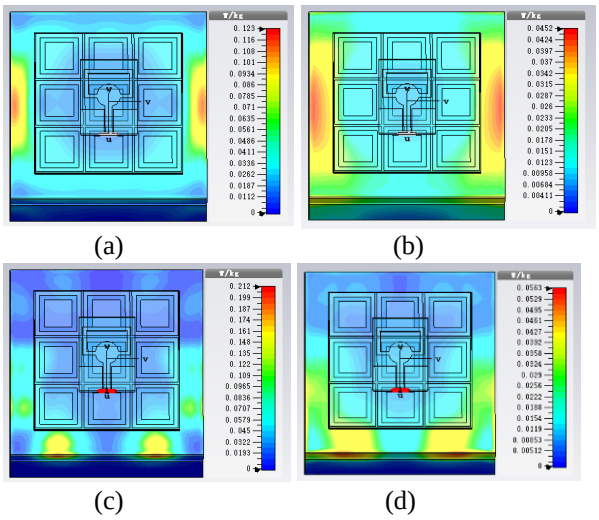

Fig. 11. Simulated SAR values for antennas with EBG. (a) 2.4 GHz, 1 g standard; (b) 2.4 GHz, 10 g standard; (c) 5.8 GHz, 1 g standard; (d) 5.8 GHz, 10 g standard.

The SAR value is crucial in understanding the effect of antenna radiation on the human body. There are two international SAR standards: one is the American standard, the other is the European standard. For the formed, enforced by the Federal Communications Commission (FCC), the threshold is 1.6 W / kg averaged over 1 g of tissue. For the latter, enforced by the International Electrotechnical Commission (IEC), the threshold is 2 W / kg averaged over 10 g of tissue [22-23]. Thus, the antennas for wearable applications must be carefully designed as complying with this regulation. To evaluate the SAR value of the antenna, a three-layer human tissue with a size of 90 × 90 × 33 mm was modeled in the CST Microwave Studio. In specific, skin, muscle, and fat tissues with a thickness of 2 mm, 8 mm, and 23 mm are used [24]. The dielectric characteristics of the

human tissue model at the frequencies of 2.4 GHz and 5.8 GHz are shown in Table 1 and Table 2, respectively. The antenna with and without the EBG structure was placed 2 mm above the human tissue for SAR analysis.

Table 4: Compare with paper on wearable antennas based on EBG or AMC

Ref.	Dimensions (mm^2)	Bandwith (GHz)	Peak Gain (dBi)	Size Comparison
[14]	200 × 200	2.45 (9.85%)	2.42	840.2%
[17]	147 × 147	2.45 (37.00%)	3.58	453.9%
		5.8 (5.04%)	6.08	
[16]	130.8 × 130.8	1.55 (1.84%)	5.1	359.3%
		2.45 (0.736%)	5.03	
[18]	124 × 124	2.45 (2.04%)	6.0	322.9%
[15]	100 × 100	3.65 (6.5%)	8.0	210.0%
		5.4 (6.5%)	8.0	
[12]	81 × 81	2.45 (14.7%)	7.3	137.8%
[19]	60 × 60	2.45 (18.4%)	6.5	75.6%
Work	69 × 69	2.45 (3.7%)	7.0	100%
		5.8 (28%)	9.1	

Figure 10 shows the SAR values of the antenna without the EBG structure. Under the 1 g standard, the SAR value of the antenna is 4.96 W / kg at 2.4 GHz and 10.9 W / kg at 5.8 GHz. For the 10 g standard, the values change to 2.6 W / kg at 2.4 GHz and 3.19 W / kg at 5.8 GHz. It should be noted that these values violate both American and European standards. Figure 11 shows the SAR values of the antenna with the EBG structure. Under the 1g standard, the SAR value reduces to 0.123 W / kg at 2.4 GHz and 0.212 W / kg at 5.8 GHz, which are respectively 97.5% and 98.1% lower than that of the antenna without the EBG structure. Under the 10g standard, the SAR value reduces to 0.0452 W / kg at 2.4 GHz and 0.0563 W / kg at 5.8 GHz, which are respectively 98.3% and 98.2% lower than that of the antenna without the EBG structure. As expected, these results validated that the EBG can reduce the SAR value of the monopole antenna. This is because the EBG changes the monopole antenna's radiation from omnidirectional to unidirectional, surpassing the surface electromagnetic waves to pass through the substrate, not the human body. Table 3, listing the SAR values studied in this paper, reveals that the antenna adopting the EBG has a very low SAR value, which complies with both American and European standards.

VI. CONCLUSION

In this paper, a dual-band wearable monopole antenna with a EBG structure was proposed. The antenna has small size and high gain characteristics compared to the Table 4 measure configurations reported for wearable applications. The proposed antenna has a working bandwidth of 2.40-2.49 GHz (3.70%) at 2.45 GHz a gain of 7.0 dBi. The bandwidth at 5.8 GHz rarely reaches to 4.85-6.50 GHz (28.9%), where the gain is approximately 9.1 dBi at 5.8 GHz. The EBG structure not only isolates the antenna from the human body but also improves the radiation gain compared to the monopole antennas without the EBG structure. More specifically, it increases the monopole antenna front-to-back ratio (FBR) by 18.2 dB (at 2.45 GHz) and 19.8 dB (at 5.8 GHz) and drops the SAR value more than 97.5%. Furthermore, it is shown that realistic human body loading have a small effect on antenna performance. Therefore, it is validated that the proposed antenna has a strong potential for wearable applications.

REFERENCES

[1] T. H. Nguyen, T. L. H. Nguyen, and T. P. Vuong, "A printed wearable dual band antenna for remote healthcare monitoring device," *2019 IEEE-RIVF International Conference on Computing and Communication Technologies (RIVF)*, 1-5, Danang, Vietnam, Mar. 2019.

[2] Y. Liao, M. S. Leeson, and M. D. Higgins, "A communication link analysis based on biological implant wireless body area networks." *Applied Computational Electromagnetics Society Journal*, pp. 619-628, June 2016.

[3] D. Ferreira, P. Pires, R. Rodrigues, and R. F. Caldeirinha, "Wearable textile antennas: Examining the effect of bending on their performance," *IEEE Antennas and Propagation Magazine*, vol. 59, no. 3, pp. 54-59, June 2017.

[4] M. I. Hossain, M. R. I. Faruque, and M. T. Islam, "A new design of cell phone body for the SAR reduction in the human head," *Applied Computational Electromagnetics Society Journal*,

pp. 792-798, July 2015.

[5] W. El Hajj, C. Person, and J. Wiart, "A novel investigation of a broadband integrated inverted-F antenna design application for wearable antenna," *IEEE Transactions on Antennas and Propagation*, vol. 62, no. 7, pp. 3843-3846, Apr. 2014.

[6] P. Saha, D. Mitra, and S. K. Parui, "A frequency and polarization agile disc monopole wearable antenna for medical applications," *Radioengineering*, pp. 74-80, Jan. 2020.

[7] M. R. Haraty, M. Naser-Moghadasi, A. A. Lotfi-Neyestanak, and A. Nikfarjam, "Transparent flexible antenna for uwb applications," *Applied Computational Electromagnetics Society Journal*, pp. 1426-1430, Dec. 2016.

[8] A. Kashkool, S. Yahya, H. Al-Rizzo, A. Al-Wahhamy, and A. A. Issac, "On the design and simulation of antennas on ultra-thin flexible substrates," *Applied Computational Electromagnetics Society Journal*, pp. 798-801, July 2018.

[9] Y. J. Li, Z. Y. Lu, and L. S. Yang, "CPW-fed slot antenna for medical wearable applications," *IEEE Access*, vol. 7, pp. 42107-42112, July 2019.

[10] Z. Hamouda, J. L. Wojkiewicz, A. A. Pud, L. Kone, S. Bergheul, and T. Lasri, "Flexible UWB organic antenna for wearable technologies application," *IET Microwaves, Antennas & Propagation*, vol. 12, no. 2, pp. 160-166, Dec. 2017.

[11] J. Trajkovikjand and A. K. Skrivervik, "Diminishing SAR for wearable UHF antennas," *IEEE Antennas and Wireless Propagation Letters*, vol. 14, pp. 1530-1533, Nov. 2014.

[12] G. P. Gao, B. Hu, S. F. Wang, and C. Yang, "Wearable circular ring slot antenna with EBG structure for wireless body area network," *IEEE Antennas and Wireless Propagation Letters*, vol. 17, no. 3, pp. 434-437, Jan. 2018.

[13] J. Wu and B. N. Li, "Development of a magneto inductive lens for magnetic resonance imaging," *IEEE Instrumentation and Measurement Magazine*, pp. 56-60, June 2017.

[14] H. Lago, P. J. Soh, M. F. Jamlos, N. Shohaimi, S. Yan, and G. A. Vandenbosch, "Textile antenna integrated with compact AMC and parasitic elements for WLAN/WBAN applications," *Applied Physics A*, vol. 122, no. 12, pp. 1059-1065, Nov. 2016.

[15] S. Karamzadeh and V. Rafiei, "Dual-band antenna modification by using dual bad EBG structure for WLAN/WiMAX applications," *Journal of Instrumentation*, 1-8, Apr. 2020.

[16] K. N. Paracha, S. K. A. Rahim, P. J. Soh, M. R. Kamarudin, K. G. Tan, Y. C. Lo, and M. T. Islam, "A low profile, dual-band, dual polarized antenna for indoor/outdoor wearable application," *IEEE Access*, vol. 7, pp. 33277-33288, Feb. 2019.

[17] M. N. Ramli, P. J. Soh, M. F. Jamlos, H. Lago, N. M. Aziz, and A. A. Al-Hadi, "Dual-band wearable fluidic antenna with metasurface embedded in a PDMS substrate," *Applied Physics A*, vol. 123, no. 2, pp. 149-156, Feb. 2017.

[18] A. Alemaryeen and S. Noghanian, "AMC integrated textile monopole antenna for wearable applications," *Applied Computational Electromagnetics Society Journal*, pp. 612-618, June 2016.

[19] G. Gao, S. Wang, R. Zhang, C. Yang, and B. Hu, "Flexible ebg-backed pifa based on conductive textile and pdms for wearable applications," *Microwave and Optical Technology Letters*, pp. 1733-1741, Apr. 2020.

[20] S. S. Bhatia and J. S. Sivia, "A novel design of circular monopole antenna for wireless applications," *Wireless Personal Communications: An International Journal*, pp. 1153-1161, Dec. 2016.

[21] S. Kim, Y. J. Ren, H. Lee, A. Rida, S. Nikolaou, and M. M. Tentzeris, "Monopole antenna with inkjet-printed ebg array on paper substrate for wearable applications," *IEEE Antennas and Wireless Propagation Letters*, pp. 663-666, Nov. 2012.

[22] H. M. Madjar, "Human radio frequency exposure limits: An update of reference levels in Europe, USA, Canada, China, Japan and Korea," *International Symposium on Electromagnetic Compatibility*, pp. 467-473, Nov. 2016.

[23] M. A. B. Mazady, G. Schmid, R. Uberbacher, and M. Ali, "SAR induced by low and high directivity antenna apertures at distances greater than 25 mm from the body," *Applied Computational Electromagnetics Society Journal*, vol. 30, no. 9, pp. 940-951, Sep. 2015.

[24] M. A. Stuchly and S. S. Stuchly, "Dielectric properties of biological substances-tabulated," *Journal of Microwave Power*, vol. 15, no. 1, pp. 19-25, Jan. 1980.